HHS Public Access

Author manuscript

J Craniofac Surg. Author manuscript; available in PMC 2016 March 01.

Published in final edited form as:

J Craniofac Surg. 2015 March ; 26(2): e148–e153. doi:10.1097/SCS.0000000000001383.

Graded Porous β-TCP Scaffolds Enhance Bone Regeneration in Mandible Augmentation

Jingwen Yang[1], **Yunqing Kang**[2], **Christopher Browne**[2], **Ting Jiang**[1,*], and **Yunzhi Yang**[2,3,*]

[1]Department of Prosthodontics, Peking University School and Hospital of Stomatology, 22# Zhong Guan Cun South Road, Beijing 100081, China

[2]Department of Orthopedic Surgery, Stanford University, Stanford, CA, 94305, USA

[3]Department of Materials Science and Engineering, Stanford University, Stanford, CA, 94305, USA

Abstract

Bone augmentation requires scaffold to promote forming of natural bone structure. Currently most of the reported bone scaffolds are porous solids with uniform pores. The aim of the present study is to evaluate the effect of a graded porous β-tricalcium phosphate scaffolds on alveolar bone augmentation. Three groups of scaffolds were fabricated by a template-casting method: (1) graded porous scaffolds with large pores in the center and small pores at the periphery; (2) scaffolds with large uniform pores; (3) scaffolds with small uniform pores. Bone augmentation on rabbit mandible were investigated by micro-CT, sequential fluorescent labeling, and histological examination three months after implantation. The result present that all the scaffold groups maintain their augmented bone height after three-month observation, while the auto-grafting group present an obvious bone resorption. Micro-CT reveals the graded porous group has significantly greater volume of new bone ($p<0.05$) and similar bone density compared to the uniform pores groups. Bone substance distribute unevenly in all the three experimental groups. Greater bone volume can be observed in the area closer to the bone bed. The sequential fluorescent labeling observation reveals robust bone regeneration in the first month and faster bone growth in the graded porous scaffold group than that in the large porous scaffold group. Histological examinations confirm bone structure in the aspect of distribution, activity, and maturity. We conclude that graded porous designed biodegradable β-tricalcium phosphate scaffolds is beneficial to promote bone augmentation in the aspect of bone volume.

Keywords

Bone regeneration; Graded pore size; β-TCP; Bone augmentation

[*]Corresponding author: Ting Jiang, DDS, PhD, Professor, Department of Prosthodontics, School and Hospital of Stomatology, Peking University, 22 South Ave. Zhongguancun, Haidian, Beijing 100081, China. Tel: 86-10-82195348, 5519, tingright@gmail.com. Yunzhi Yang, PhD, Associate Professor, Department of Orthopedic Surgery, Stanford University, 300 Pasteur Drive, Edwards R155, Stanford, CA 94305, Mail code: 5341, Tel: 650-723-0772 (Office), 650-725-8698 (Lab), Fax: 650-721-5404, ypyang@stanford.edu.

1. Introduction

Titanium dental implants are rapidly becoming a routine procedure in today's dentistry and are widely used for a variety of cases, which includes surgical replacement of lost teeth or restoration of oral function [1, 2]. A significant factor that limits the clinical application of a titanium dental implant is the restrictive necessity for alveolar bone mechanical support[3, 4]. New advances brought by bone tissue engineering, in particular by bone grafts, may surmount the current deficits of titanium dental implants.

One approach to designing bone grafts for alveolar bone augmentation or repair of critical size defects is biomimicking the chemical composition and structural features of natural bone, thus achieving similar regenerative properties [5–8]. Scaffolds fabricated with calcium phosphate ceramics such as hydroxyapatites and beta-tricalcium phosphate (β-TCP) have been shown to repair bone defects in clinical applications due to their biocompatibility and resemblance in chemistry composition to natural bone [9, 10.] Additionally, an interconnected pore structure and high porosity are essential for scaffolds, as they permit the exchange of nutrient transport within the scaffold and facilitate the ingrowth of cells and tissues. Currently most of the reported bone scaffolds are porous solids with uniform pores [11–13]. However, in nature, bone has a graded architecture. Both long bones and flat bones change spatially and gradually from a dense, stiff external structure (cortical bone) to a porous internal structure (cancellous bone) [14]. Therefore, adhering to the cues from nature, graded-based strategies can be used in design and fabrication of scaffolds for mimicking bone structure to promoting bone repair and regeneration[15, 16]. New research investigating the effect of assorted pore diameters in β-TCP scaffolds (150, 260, 510 and 1220μm) has demonstrated an inherent variance in bone formation and resorption rate amongst each group, suggesting the spatial distribution of different pore sizes directly affect bone structure of the engineered bone[17].

Creating a suitable graded porous ceramic scaffold that has adequate pore spatial distribution and interconnected pore structure has been a challenge[16]. We addressed this problem by developing a template-casting method to easily fabricate porous ceramic scaffolds with controlled spatial variation of chemistry and interconnected pore structure [18]. Also, through this method, the desirable prerequisites of shape customization and pore size distribution could be fulfilled to achieve a graded pore distribution in a spatial manner. In this study, we fabricated three groups of scaffolds: (1) graded porous scaffolds; (2) large porous scaffolds; (3) small porous scaffolds, and evaluated the effect of the scaffolds with rhBMP-2 on osteogenesis and vertical augmentation in a rabbit mandibular defect model. By analyzing the difference of generated bone in the aspects of bone volume and bone density among the groups after three months of observation, we tend to find a suitable design of bone substitute.

2. Materials and methods

2.1. Scaffold preparation

The following three groups of scaffolds with completely interconnected pores were prepared by our template-casting method[18]: (1) graded porous scaffolds (600–800 μm pores in the

center and 350–500 μm pores at the periphery); (2) large porous scaffolds (600–800 μm uniform pores); (3) small porous scaffolds (350–500 μm uniform pores). The fabrication process of the scaffolds included β-TCP slurry preparation, molding, casting, solidifying, drying, and sintering [19]. Gross and micro-CT examinations of their transverse section were performed as described previously [20]. The structural patterns of the β-TCP scaffolds were imaged as described in Figure 1. All the scaffolds were molded into cylinders with a height of 6 mm and a diameter of 8 mm. As for the graded scaffolds, the central region containing the larger pores was 4 mm in diameter, while the outer layer containing the smaller pores had a thickness of 4 mm.

2.2. Scanning electron microscopy (SEM)

Morphology of the scaffolds were observed using a scanning electron microscope (SEM, FEG-Philip XL30 ESEM, 2525 V). Prior to the observation, the samples were coated with a thin layer of Pt-Au.

2.3. In vivo study of osteogenesis ability

2.3.1. Surgical process—A total of ten male New Zealand rabbits (8 weeks, 2.5–3.0 kg) with twenty mandibular sites was used to evaluate the *in vivo* osteogenesis ability of the three groups of β-TCP scaffolds (graded pores, large pores, and small pores) loaded with rhBMP-2, one positive control group (autogenous graft), and one negative control group (identical surgery without implantation) (n=4 per group). All animal studies were performed in accordance with procedures approved by the Animal Care and Ethics Committee of Peking University Health Science Center. The scaffolds were sterilized by gamma irradiation before rhBMP-2 was applied. rhBMP-2 solution (Peprotech, USA, 100 μL) (>95% purity, 0.1 mg/ml, 10 μg per scaffold) was applied to the scaffolds. Animals were quarantined for a minimum of one week prior to experimentation and they had *ad libitum* access to standard rabbit chow and water at all times.

To start the surgical process, the rabbits were anesthetized with sodium pentobarbital (30 mg/kg) by injection into the lateral ear vein. After hair shaving, a horizontal incision(25 mm) was made over the submandibular region to expose the buccal ramus of the mandible. A bone defect (8 mm diameter, 2mm depth) was then created on the buccal ramus. Autogenous bone grafts from iliac bone(8 mm in diameter, 4mm in height) were fixed with titanium screws(1.5 mm in diameter, 8 mm in length) onto the mandible surface. The scaffolds(8 mm in diameter, 6mm in height) embedded in the defect protruded the same height with the auto-grafts did(4 mm) from the bone surface. All the blocks were covered by biodegradable membranes (Shenzhen Lando Biomaterials Co., Ltd.). For negative control group, a bone defect was created, without material implanted. The entire procedure was performed under sterile conditions. After the surgery, all rabbits received antibiotics (penicillin G, 200000 units) intramuscularly daily for 3 days. Animals were housed individually, kept in a 12 h light/dark cycle at controlled temperature (21°C) and fed *ad libitum* with standard laboratory diet.

The animals were sacrificed 3 months after the surgery with an overdose of sodium pentobarbital and the samples were prepared for examinations.

2.3.2. Fluorochrome labeling and observation—Sequential fluorochrome labeling was used to determine the onset time of mineralization, and the speed of new bone (spicule) formation. Polyfluorochrome tracers (tetracycline, alizarin red, calcein) were subcutaneously injected as indicated in Table 1. After sample processing, polyfluorochrome tracers were identified by fluorescence microscopy. Imagepro-Plus 6.0 was used to analyze the proportion of each fluorochrome labeled area. Six regions of interest were selected from each sample according to different locations within the implanted scaffolds: outside-upper (O-U), outside-middle (O-M), outside-lower (O-L), inside-upper (I-U), inside-middle (I-M), and inside-lower (I-L). The level of mineralization of each region was blindly analyzed by an examiner who was not aware of the study design.

2.3.3. Histomorphometric examination—After fixation with 10% phosphate-buffered formalin, the samples of mandibles were cut into two halves. One half of each sample was dehydrated in ethanol and then embedded in acrylic resin. The embedded blocks were trimmed by cutter and further ground to a final thickness of about 40μm. Then the hard tissue slices were stained with toluidine blue and microscopically examined (Zeiss, LSM 5 EXCITER). The other half of each sample was decalcified with 5% formic acid for 2 weeks[21], and then embedded in paraffin parallel to the sectioned surface. Serial cross sections of decalcified samples were sectioned for haematoxylin and eosin (H&E) stain, toluidine blue staining, Masson's staining, and osteocalcin (anti-osteocalcin antibody, Abcam, ab13420) with immunohistochemistry staining.

2.3.4. Micro-computed tomography (μCT) measurement—To quantify the bone regeneration in the implantation site, bone volume (BV) and bone mineral density (BMD) of each specimen were measured by micro-computed tomography (μCT) scans and analysis. All specimens were cut into rectangular prisms(1 cm^3) containing the tissue-engineered construct. Samples were examined with a Skyscan 1076 high-resolution desk-top μCT system (Skyscan®, Kontich, Belgium). Taking into account the camera definition and the source–object–camera distance, 2D images (pixel size, 8.665 μm) were obtained. The corresponding 3D images were produced by stacking all the 2D cross sections.

To study the scaffold pore size effect on bone formation, 6 regions of interest from different locations within the implanted blocks were selected, and each region was shaped into a cylinder (2 mm in diameter and 2 mm in length). After selection, an upper and lower threshold value were decided to separate the bone from other tissues, and then the bone volume (BV), tissue volume (TV), bone volume/tissue volume, and bone density were calculated and analyzed using CTAn version 1.11.8.0+ (64-bit). The bone volume (BV) was defined as the volume of newly formed bone in the selected region with a threshold between 50 and 130, and the tissue volume (TV) was defined as the overall volume in the selected region with a threshold below 130 which excluded the scaffold. We used the BV/TV as the index for new bone formation for comparison. Bone mineral density was defined as the mineral density of the newly formed bone in pores of the scaffolds.

2.4. Statistical analysis

To further compare the regeneration ability among different sites in the scaffolds, six locations in each sample were selected and analyzed. Both the bone volume and the bone mineral density were calculated. Statistics of each scaffold groups were analyzed in SPSS 17.0 software (IL, USA). Two-way ANOVA with Tukey's post-hoc test for multiple comparisons was used. The level for significance was set at $p< 0.05$.

3. Results

3.1. SEM examination

A SEM micrograph (Figure 2) of the β-TCP porous scaffolds prepared from the template-casting method shows the interconnected structure of pores. Under low magnification, graded porous scaffolds showed the change of pore sizes, from central large pores (600–800μm) to peripheral small pores (350–500μm). No cracks or delamination were observed at the interface between zones in the samples. In uniform-size scaffolds, interconnected windows in the pores were seen. Under high magnification, micropores were observed in the struts of the three types of scaffolds.

3.2. In vivo osteogenic ability

3.2.1. Polyfluorochrome labeling on non-decalcified samples—The non-decalcified hard-tissue slices showed that the height of experimental groups was stable and the scaffolds maintained their original shape (Figure 3A, 3B, 3C). On the other hand, the shape of the transplanted iliac bone changed. Although the autogenous implants were stable and integrated to bone, protruding bone appeared as a hemisphere, rather than a cylinder-like shape. Moreover, their height decreased (Figure 3D). As for the negative control, no vertical augmentation was observed, but dense tissue was formed bridging the bone defect (Figure 3E). The fluorescence of the slices showed continuous mineralization through the entire 3 months after surgery. The blue, red, and green fluorescent color indicates the newly-formed bone within the first, second or third month. The intensity and region of colors suggested the extent and location of the newly-formed bone. In the scaffold groups, the areas of blue, red, and green color regions were different, while in the control groups, all colors covered the same area when superimposed. By comparing the three colored areas in scaffold groups, we found that the blue regions (tetracycline-labeled for the newly-formed bone within the first month) were the largest and that red and green regions adjacent to the blue regions were much smaller. Our analysis showed that, the tissue area labeled for newly formed bone decreased over time (Figure 4A), and no significant difference was found between the core area and the peripheral area. The newly formed bone areas labeled in the first month were significantly greater than those in the second and third months. And the bone areas colored blue in the graded porous scaffolds were significantly larger than those in the large porous scaffolds(Figure 4B)($p<0.05$).

3.2.2. Histological evaluation—H&E staining of the samples revealed that in all the groups, implanted blocks were tightly bound and integrated to the mandible bed, and no inflammation was found in any of the samples after surgery (Figure 5). From the general view, it was obvious that the distribution of regenerated bone was uneven in the scaffolds.

For all groups, bone volume near the bone bed seemed to be greater than those far from the base area. However, all the scaffold groups demonstrated a well-formed bone structure. At the magnification of 200×, both bone tissue and soft tissue could be detected. Empty spaces interspersed in the tissues indicate areas where the scaffold was before demineralization. Immunohistochemistry staining of osteocalcin revealed active bone mineralization in all the groups, though the ranges of brown-colored tissue were different in each group (Figure 6). Toluidine blue staining of the hard tissue slices clearly demonstrated the distribution of bone tissue in blue, and the scaffold structure in black (Figure 7). The gross view of the toluidine blue staining was in accordance with that of H&E staining, characterized with uneven bone forming from the base to the top of the scaffolds. Images showed close integration between bone tissue and scaffolds. At high magnification of 100×, initimate integration was found both in the bone scaffold interface and implant bone interface. Masson's trichrome staining of all the samples presented a red color for cytoplasm, scattered with bits of blue for bone (Figure 8), which indicated wide range of bone tissue in the form of collagen. Collagen was mostly scattered around the bone lacunae.

3.2.3. μCT observation and measurements—Figure 9 shows 2D profile μCT images of the mandible explants. Comparing the coronal image series of each sample of scaffold groups, identifiable differences in pore patterns could be observed. For the graded porous scaffold group (Figure 9D), large pore scaffold group (Figure 9E), and small pore scaffold group (Figure 9F), the difference in pore diameters was obvious as designed. High density tissue deposition was observed in pores. The distribution pattern varies among different tomography slice levels.

3.2.4. Bone volume (BV) and tissue volume (TV) measurements—The BV/TV ratio was used as the most important index for new bone formation in this study. The BV/TV ratios were different among the three groups, with statistical significance as shown in Figure 10. The ratio of BV/TV in graded porous scaffolds was significantly higher than those with large pores ($p<0.01$) and small pores ($p<0.05$), suggesting much greater new bone formation. No statistical difference was found between the two groups with uniform pores (Figure 10A). In consistence with H&E staining, the ratio of BV/TV of different regions presented a slight decreasing trend from bottom to top of the blocks. Statistical differences were found not only between the outside-upper and outside-lower areas, but also the central-upper and outside-lower areas(Fig. 11C). The bone density showed no significant difference among the groups (Fig. 11B) or between different regions (Fig. 11D).

4. Discussion

With the purpose of improving the osteogenic potential of β-TCP porous ceramics, we evaluated bone enhancement of porous scaffold with the addition of growth factor in bone defect models[22]. Porous scaffolds have been studied for decades, the uniform pore architecture of scaffolds faces a significant challenge in inducing the growth of new tissue in the way of natural bone acts [23–26]. The architectural motif of natural bone can be described as having a stiff, dense external layer of cortical bone, transitioning to a thin and porous cancellous bone internally[15]. There have been attempts to establish a fabrication method to manufacture a kind of scaffold that is both graded and is highly interconnected[27–30]. Graded

porous scaffolds have been proven to be advantageous compared with uniform pore design in both ectopic and orthotopic [31, 32] osteogenesis, overcoming the current limitations associated with uniform pore design. The purpose of this study was to demonstrate the advantage of the designed graded porous scaffolds fabricated by a template-casting technique on bone augmentation in orthotopic bone defect.

Our *in vivo* study with New Zealand rabbits confirmed our hypothesis that the graded porous scaffold loaded with rhBMP-2 promoted bone augmentation at a higher rate compared to scaffolds with uniform pore sizes with the same loading of rhBMP-2 in orthotopic osteogenesis. μCT analysis revealed superior bone volume augmentation in the graded porous scaffold group, with no decrease in bone mineral density compared to uniform-size scaffolds, which excluded the possibility of impaired bone quality. The decreasing trend of bone volume from the base to the top of the scaffolds implied blood supply effect on bone regeneration. The obvious difference of augmented bone height between the experimental groups and the positive control group further demonstrated the advantages of engineered bone over autogenous iliac grafts in the aspect of bone configuration, which proved the mechanical support provided by the scaffold can withstand pressure from the surrounding soft tissue, maintaining a stable bone height during the three month implantation period, while iliac grafts underwent a dramatic reconstruction which lead to a bone height reduction. Although bone tissue in scaffolds presented an uneven distribution and different degrees of maturity, the structure of the mature part was familiar with that of the natural bone in the positive control group, such as typical lamellar bone mingled with woven bone, spotted osteocytes and Haversian canals. As for the immature part, experiments with longer observing period need to be conducted. Masson's staining revealed the maturity of the engineered tissue in most of the observed areas, while active osteogenesis appeared to be around the fringe, indicating the presence of a stable bone structure with active growth.

The poly-fluorescent labeling is to visualize the process of new bone formation by identifying mineralized tissue during the drug injection period[33]. Since the injecting time interval of the three labeling drugs was the same, the larger the labeled areas are, the larger area the mineralized bone occupied. In our experiments, the bone growth in the first month was the fastest. And the difference of regenerated bone between the graded porous scaffolds and the uniform scaffolds had already emerged during this time, which provide further proof of the improved bone regeneration in the graded porous scaffolds, though the difference is not as significant as the μCT examination due to the limitation of information sample slices could ever offer. During the following two months, the bone formation/augmentation declined. Similar observation was found in other ectopic and orthotopic animal models as well[34, 35]. The surgically created bone defect control groups showed little regeneration as evidenced by the lack of calcium ion deposition in the implantation area. In our study, the intrinsic mechanism of the advantage of graded porous scaffolds seems to be various rather than single-effect. Since no significant difference was found between the core area and the peripheral area in this study, we believe that the graded scaffold act as a unique, single functional unit that the different configuration of the scaffold cause interstitial fluid diffusion changes and scaffold degradation profile changes, which lead to the different cell adhesion and different cell behavior as a response to the scaffold degradation. Considering

the living organism is such a complex system that a graded porous design is far from bio-mimicking, further investigations on scaffolds development about scaffold degradation, growth factor release and blood supply improvement should be considered. However, based on our study on osteogenesis of porous scaffolds, the graded porous design could be proved to be beneficial in bone augmentation in orthotopic osteogenesis.

Acknowledgments

This study was supported by grants from Beijing Natural Science Foundation (7133255), NIH R01DE021468 (NIDCR), NIH R01AR057837 (NIAMS), and DOD W81XWH-10-1-0966 (PRORP).

References

1. Shimono K, Oshima M, Arakawa H, et al. The effect of growth factors for bone augmentation to enable dental implant placement: A systematic review. Japanese Dental Science Review. 2010; 46:43–53.
2. Davo R, Malevez C, Rojas J. Immediate function in the atrophic maxilla using zygoma implants: a preliminary study. J Prosthet Dent. 2007; 97:S44–51. [PubMed: 17618933]
3. Cawood JI, Howell RA. Reconstructive preprosthetic surgery. I. Anatomical considerations. Int J Oral Maxillofac Surg. 1991; 20:75–82. [PubMed: 2051053]
4. McAllister BS, Haghighat K. Bone augmentation techniques. J Periodontol. 2007; 78:377–396. [PubMed: 17335361]
5. Block MS, Kent JN. Long-term radiographic evaluation of hydroxylapative-augmented mandibular alveolar ridges. Journal of Oral and Maxillofacial Surgery. 1984; 42:793–796. [PubMed: 6094773]
6. Jeon I-S, Heo M-S, Han K-H, et al. Vertical ridge augmentation with simultaneous implant placement using β-TCP and PRP: A report of two cases. Journal of Oral and Maxillofacial Surgery, Medicine, and Pathology.
7. Kent JN, Quinn JH, Zide MF, et al. Alveolar ridge augmentation using nonresorbable hydroxylapatite with or without autogenous cancellous bone. Journal of Oral and Maxillofacial Surgery. 1983; 41:629–642. [PubMed: 6312003]
8. Wang S, Zhang Z, Zhao J, et al. Vertical alveolar ridge augmentation with β-tricalcium phosphate and autologous osteoblasts in canine mandible. Biomaterials. 2009; 30:2489–2498. [PubMed: 19147220]
9. Chow LC. Calcium phosphate cements. Monogr Oral Sci. 2001; 18:148–163. [PubMed: 11758446]
10. LeGeros RZ. Calcium phosphates in oral biology and medicine. Monogr Oral Sci. 1991; 15:1–201. [PubMed: 1870604]
11. Eggli PS, Muller W, Schenk RK. Porous hydroxyapatite and tricalcium phosphate cylinders with two different pore size ranges implanted in the cancellous bone of rabbits. A comparative histomorphometric and histologic study of bony ingrowth and implant substitution. Clin Orthop Relat Res. 1988:127–138. [PubMed: 2838207]
12. Schliephake H, Neukam FW, Klosa D. Influence of pore dimensions on bone ingrowth into porous hydroxylapatite blocks used as bone graft substitutes. A histometric study. Int J Oral Maxillofac Surg. 1991; 20:53–58. [PubMed: 1850445]
13. Gauthier O, Bouler JM, Aguado E, et al. Macroporous biphasic calcium phosphate ceramics: influence of macropore diameter and macroporosity percentage on bone ingrowth. Biomaterials. 1998; 19:133–139. [PubMed: 9678860]
14. Sah RL. Interface and bulk regions in the repair, regeneration, and replacement of articular cartilage. J Musculoskelet Neuronal Interact. 2004; 4:393–395. [PubMed: 15758275]
15. Pompe W, Worch H, Epple M, et al. Functionally graded materials for biomedical applications. Materials Science and Engineering: A. 2003; 362:40–60.
16. Muthutantri A, Huang J, Edirisinghe M. Novel preparation of graded porous structures for medical engineering. Journal of The Royal Society Interface. 2008; 5:1459–1467.

17. von Doernberg MC, von Rechenberg B, Bohner M, et al. In vivo behavior of calcium phosphate scaffolds with four different pore sizes. Biomaterials. 2006; 27:5186–5198. [PubMed: 16790273]
18. Liu Y, Kim JH, Young D, et al. Novel template-casting technique for fabricating beta-tricalcium phosphate scaffolds with high interconnectivity and mechanical strength and in vitro cell responses. J Biomed Mater Res A. 2010; 92:997–1006. [PubMed: 19296544]
19. Kang Y, Kim S, Khademhosseini A, et al. Creation of bony microenvironment with CaP and cell-derived ECM to enhance human bone-marrow MSC behavior and delivery of BMP-2. Biomaterials. 2011; 32:6119–6130. [PubMed: 21632105]
20. Jason A, Berdick RLM. Biomaterials for Tissue Engineering Application: A Review of the Past and Future Trends. Biomaterials for Tissue Engineering. 2012:29.
21. Frank JD, Balena R, Masarachia P, et al. The effects of three different demineralization agents on osteopontin localization in adult rat bone using immunohistochemistry. Histochemistry. 1993; 99:295–301. [PubMed: 8500993]
22. Lim HP, Mercado-Pagan AE, Yun KD, et al. The effect of rhBMP-2 and PRP delivery by biodegradable beta-tricalcium phosphate scaffolds on new bone formation in a non-through rabbit cranial defect model. J Mater Sci Mater Med. 2013; 24:1895–1903. [PubMed: 23779152]
23. Sanz-Herrera JA, Garcia-Aznar JM, Doblare M. On scaffold designing for bone regeneration: A computational multiscale approach. Acta Biomater. 2009; 5:219–229. [PubMed: 18725187]
24. Drury JL, Mooney DJ. Hydrogels for tissue engineering: scaffold design variables and applications. Biomaterials. 2003; 24:4337–4351. [PubMed: 12922147]
25. Alsberg E, Kong HJ, Hirano Y, et al. Regulating bone formation via controlled scaffold degradation. J Dent Res. 2003; 82:903–908. [PubMed: 14578503]
26. Park SH, Gil ES, Kim HJ, et al. Relationships between degradability of silk scaffolds and osteogenesis. Biomaterials. 2010; 31:6162–6172. [PubMed: 20546890]
27. Hutmacher DW. Scaffold design and fabrication technologies for engineering tissues—State of the art and future perspectives. Journal of Biomaterials Science. 2001; 12:15.
28. Freed LE, Vunjak-Novakovic G, Biron RJ, et al. Biodegradable polymer scaffolds for tissue engineering. Biotechnology. 1994; 12:5.
29. Ma PX, RZ. Microtubular architecture of biodegradable polymer scaffolds. Journal of Biomedical Materials Research. 2001; 56:8.
30. Mooney DJ, Organ G, Vacanti JP, et al. Design and fabrication of biodegradable polymer devices to engineer tubular tissues. Cell Transplantation. 1994; 3:8.
31. Kuboki Y, Jin Q, HT. Geometry of carriers controlling phenotypic expression in BMP-induced osteogenesis and chondrogenesis. The Journal of Bone and Joint Surgery. 2001; 83:11.
32. Lan Levengood SK, Polak SJ, Poellmann MJ, et al. The effect of BMP-2 on micro- and macroscale osteointegration of biphasic calcium phosphate scaffolds with multiscale porosity. Acta Biomater. 2010; 6:9.
33. van Gaalen SM, Kruyt MC, Geuze RE, et al. Use of fluorochrome labels in in vivo bone tissue engineering research. Tissue Eng Part B Rev. 2010; 16:209–217. [PubMed: 19857045]
34. Hernández A, Sánchez E, Soriano I, et al. Material-related effects of BMP-2 delivery systems on bone regeneration. Acta Biomater. 2012; 8:11.
35. Patel ZS, Yamamoto M, Ueda H, et al. Biodegradable gelatin microparticles as delivery systems for the controlled release of bone morphogenetic protein-2. Acta Biomater. 2008; 4:13.

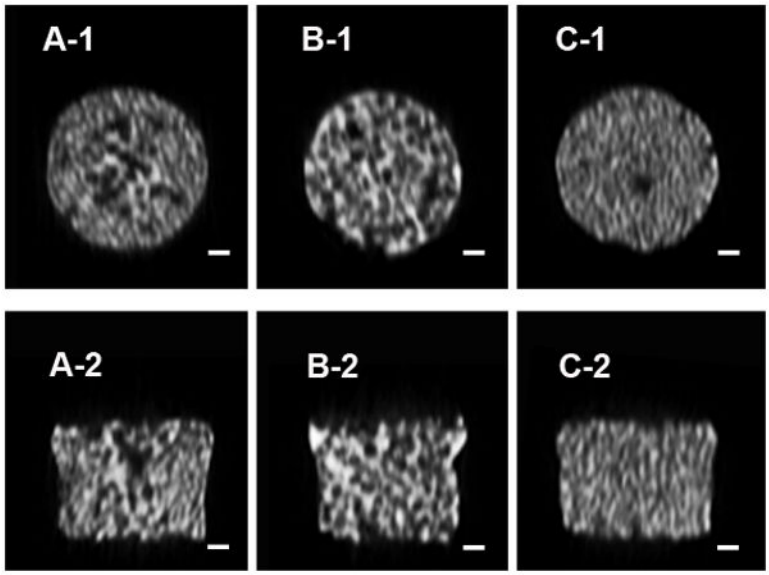

Figure 1.
μCT images. A, B, C show images of the graded porous scaffolds(GP), the large pore scaffolds(LP), and the small pore scaffolds (SP). Scale bars = 1000 μm.

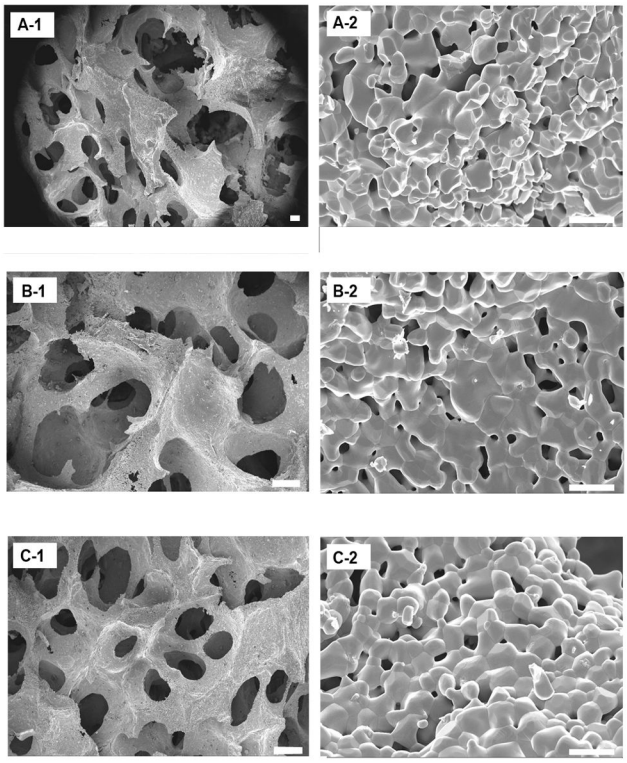

Figure 2.

Scanning electron microscopy examination of the three kinds of scaffolds. A, B, and C show images of GP, LP, and SP, respectively. A-1 shows the junction between large and small pore regions. A-2, B-2, and C-2 show high-magnification scans of their respective surfaces. Scale bars = 200 μm for A-1, B-1, and C-1; scale bars = 10 μm for A-2, B-2, and C-2.

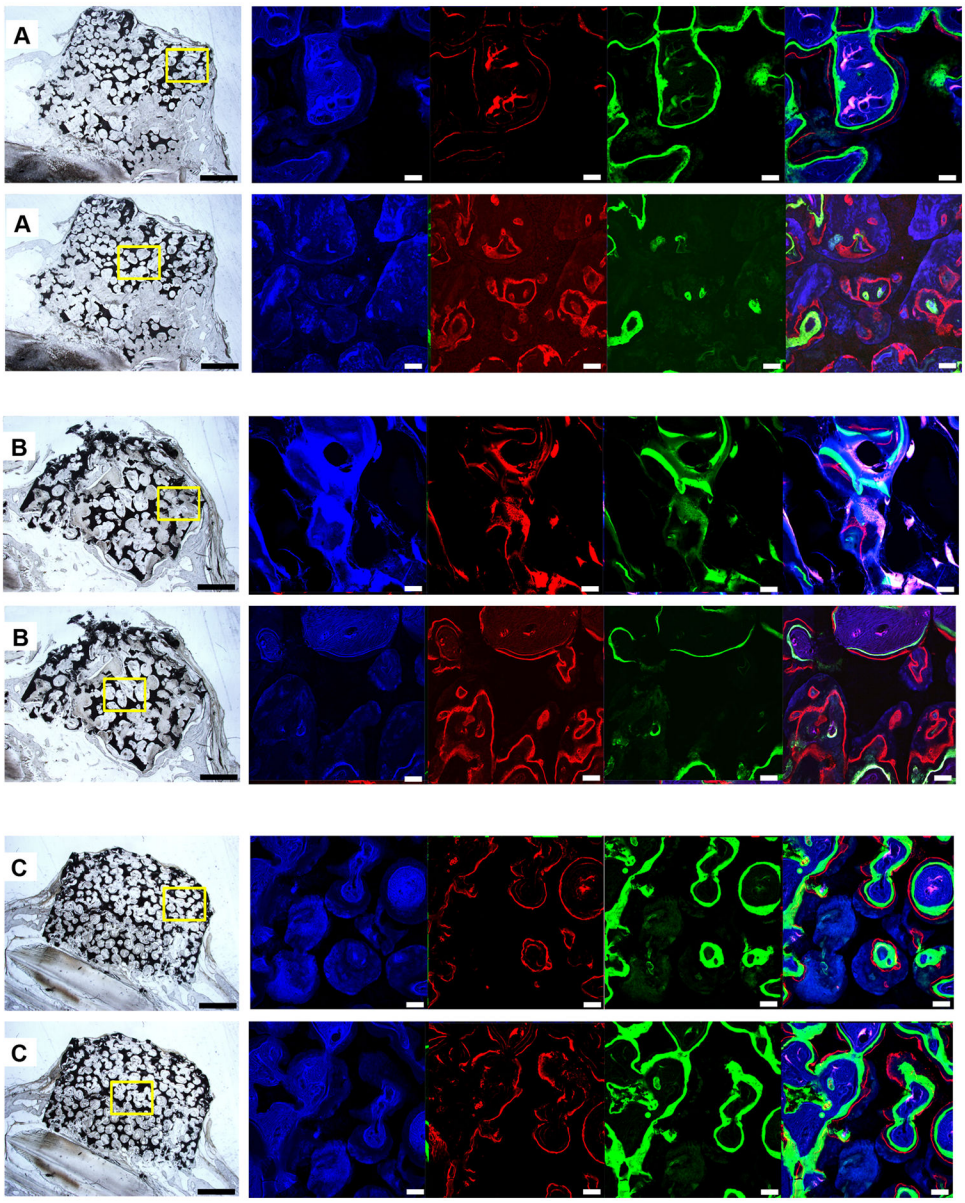

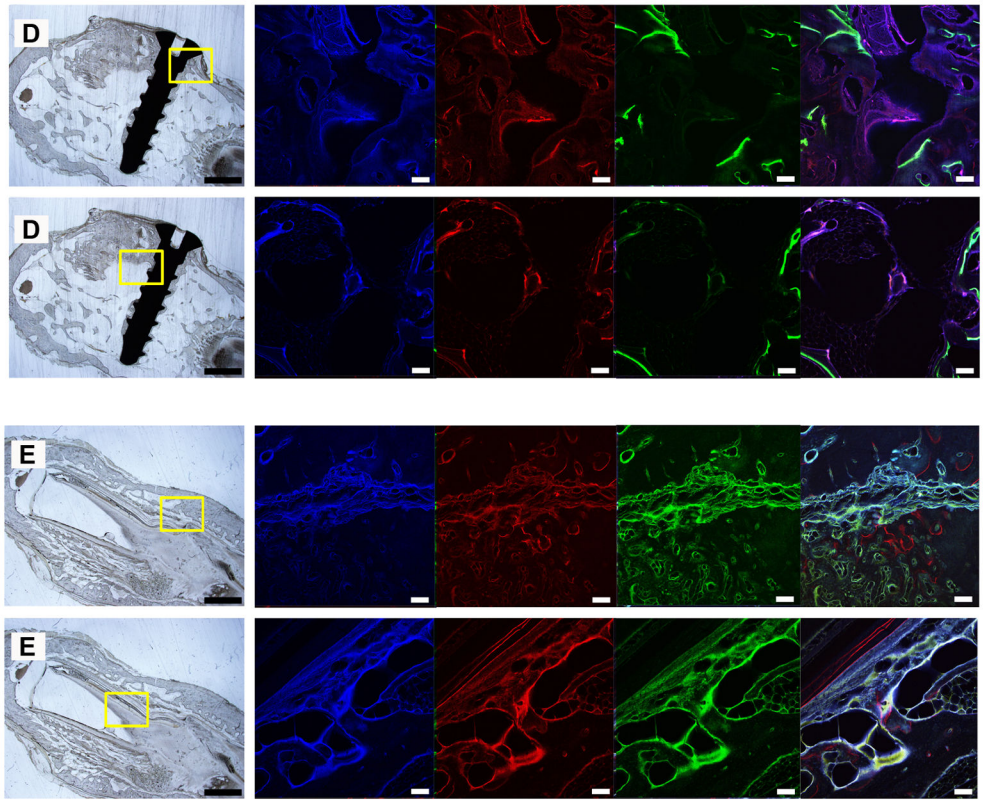

Figure 3.

Fluorescent labeling of new bone formation over time. A, B, C, D, and E show images of GP, LP, SP, positive control group, and negative control group. In each sample, 2 fluorescent labeling areas are presented, one in the center of the slices, the other in the outer ring of the slices. Each result includes a general view of the abrasive slice and a series of fluorescent labeled images captured after excitation at different wavelengths. There are 4 fluorescent labeled images in each series. Images in blue, red, and green present the calcified tissue in the first, second, and third month, respectively. The last column in each series shows the computer generated merged images. Scale bars = 1000 μm in abrasive slices; scale bars = 100 μm in fluorescent labeled images.

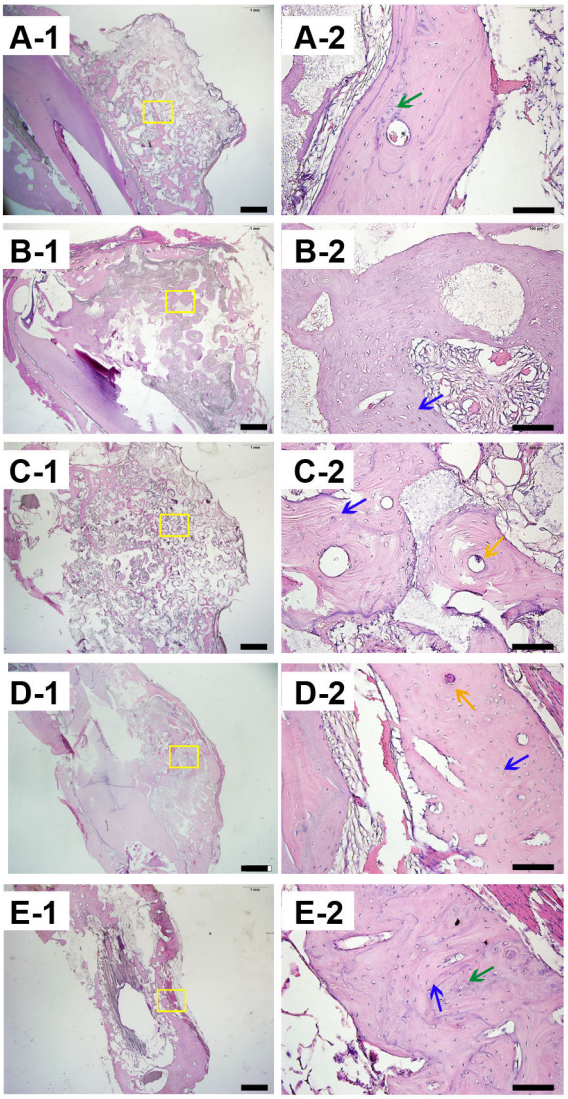

Figure 4.

Quantitative analysis of fluorescent labeled areas in each groups(GP, SP, and LP). A show the areas in the first, second and third month. The violet lines present areas in the core of scaffolds(I-U, I-M, I-L), while the green lines present the area in the periphery of the scaffolds(O-U, O-M, O-L). B show the statistic analysis result in the first month.

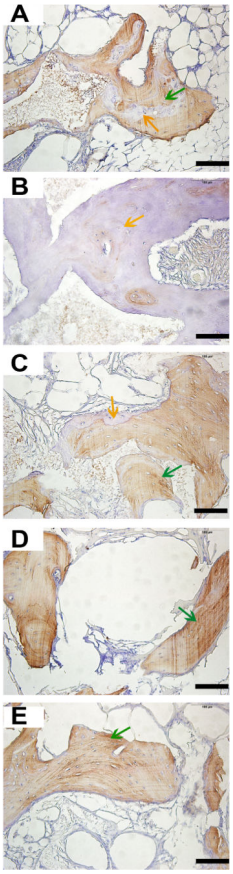

Figure 5.

Hemotoxylin and eosin (H&E) staining of the decalcified samples. A, B, C, D, and E show images of GP, LP, SP, positive control group, and the negative control group. Blue arrows indicate bone matrix spotted with osteocytes, green arrows indicate osteoid, and yellow arrows indicate Haversian canals. Scale bars = 1000 μm in A-1, B-1, C-1, D-1 and E-1; Scale bars = 100 μm in A-2, B-2, C-2, D-2 and E-2.

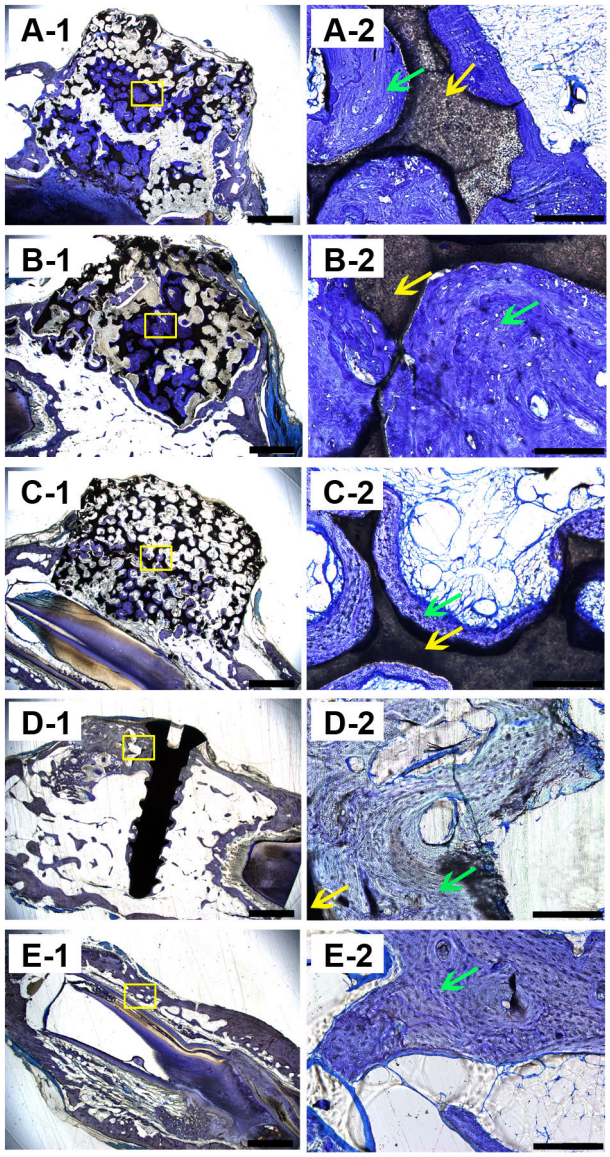

Figure 6.

Immunohistochemistry staining of osteocalcin. A, B, C, D, and E show images of GP, LP, SP, positive control group, and the negative control group. Green arrows indicate the mineralized tissue and yellow arrows indicate the tissue not mineralized. Scale bars = 100 μm.

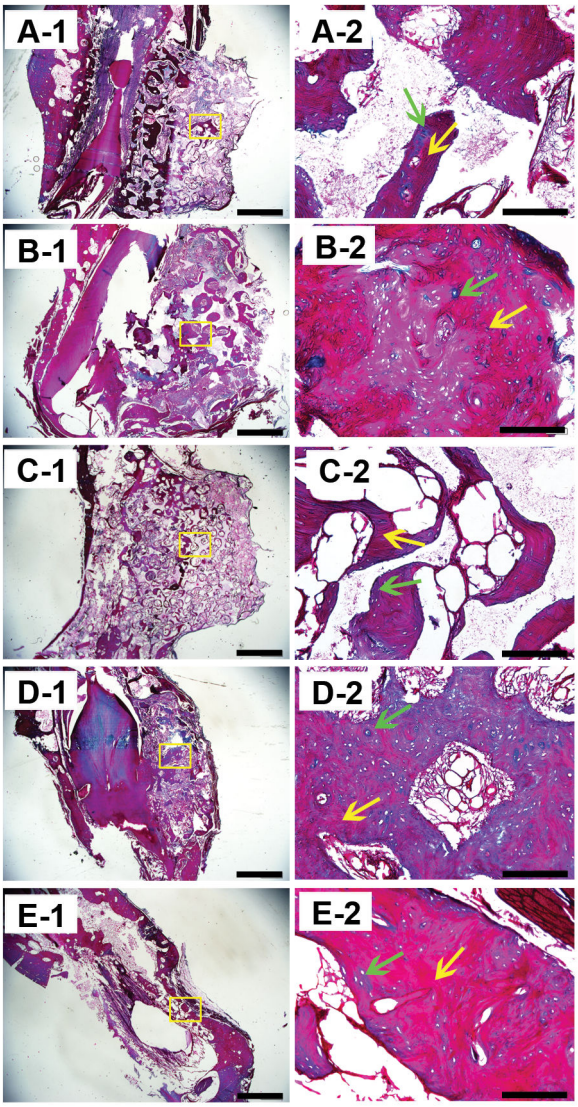

Figure 7.

Toluidine blue staining of the hard tissue slices of all the samples. A, B, C, D, and E show images of GP, LP, SP, positive control group, and the negative control group. Green arrows indicate bone tissue and yellow arrows indicate the scaffolds. Scale bars = 1000 μm in A-1, B-1, C-1, D-1 and E-1; Scale bars = 100 μm in A-2, B-2, C-2, D-2 and E-2.

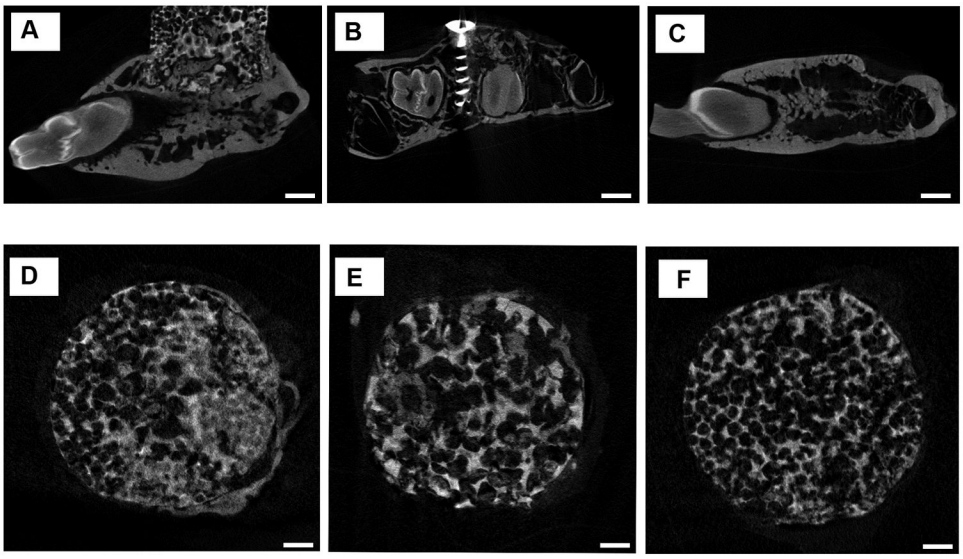

Figure 8.

Masson's trichrome staining of the samples. A, B, C, D, and E show images of GP, LP, SP, positive control group, and the negative control group. Green arrows indicate the immature bone tissue and yellow arrows indicate the mature bone tissue. Scale bars = 1000 μm in A-1, B-1, C-1, D-1 and E-1; Scale bars = 100 μm in A-2, B-2, C-2, D-2 and E-2.

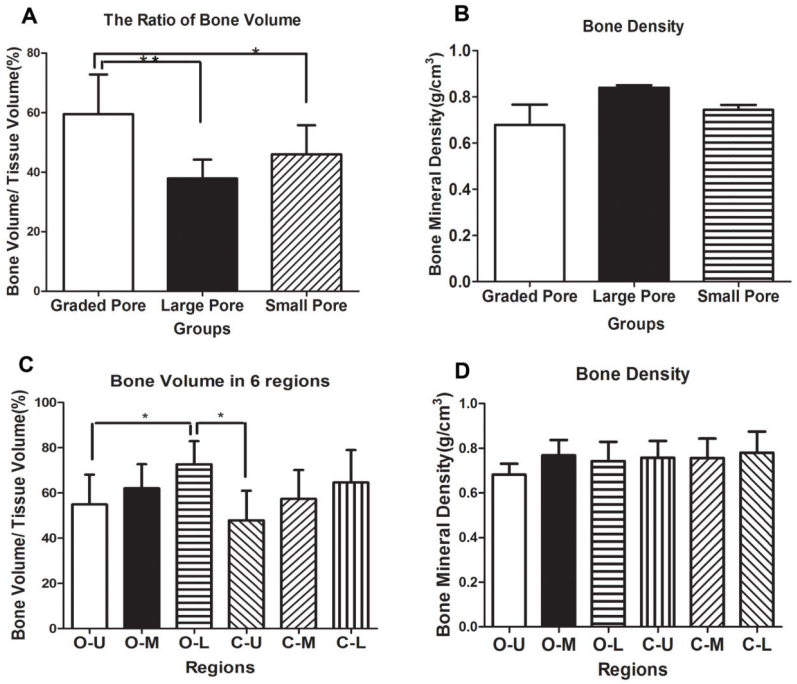

Figure 9.

μCT sagittal images of samples of augmented mandibles. A is the experimental group; B is the positive control group; C is the negative control group. D, E, and F are the micro CT coronal images of the samples of three experimental groups. D shows GP group, E shows LP group, and F shows SP group. Scale bars = 1000 μm.

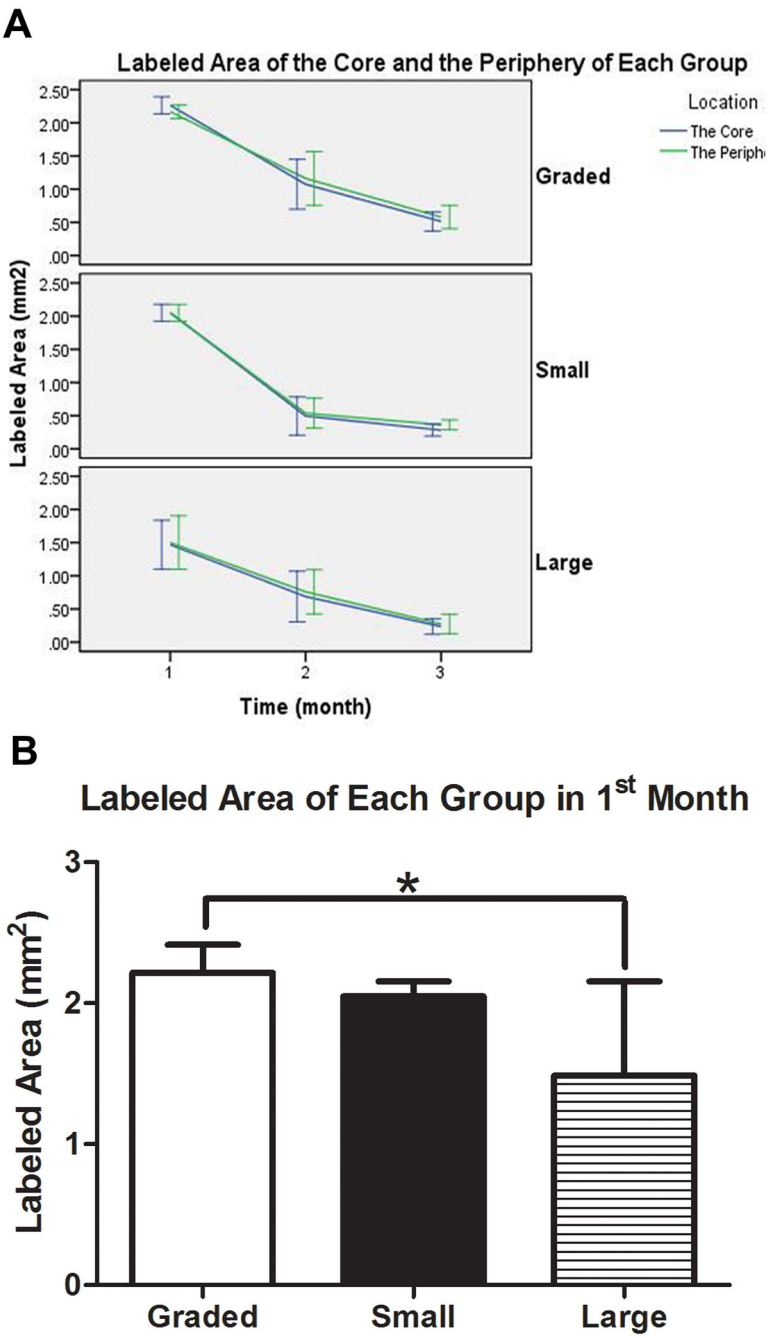

Figure 10.

μCT quantitative analysis of newly-formed bone. A and B show the statistical analysis of μCT measurements of the augmented mandibles in three experimental groups in terms of bone volume/tissue volume and bone mineral density. C and D show the statistical analysis of μCT measurement of the augmented mandibles in six different areas in the scaffolds.

Table 1

Injection schedule and dosage of polyfluorochrome markers

Time [days]	Substance	Doses [mg/kg]
14	Tetracycline	60
44	Alizarin Red ($C_{14}H_8O_4$)	30
74	Calcein ($C_30H_{26}N_4O_{13}$)	10